A&A, 707, A177 (2026)
https://doi.org/10.1051/0004-6361/202557410

Astronomy & Astrophysics

Sulphur isotopic composition of comet 67P/Churyumov-Gerasimenko: Constraints from $C^{34}S_2$ measured by ROSINA

Antea C. Doriot[1,⋆], Kathrin Altwegg[1], Robin Bonny[1], Michael R. Combi[2], Stephen Fuselier[3,4], Nora Hänni[1], Johan De Keyser[5], Daniel Müller[1], Martin Rubin[1], and Susanne F. Wampfler[6]

[1] Space Research and Planetary Sciences, Physikalisches Institut, University of Bern, Sidlerstrasse 5, 3012 Bern, Switzerland
[2] Department of Climate, Space Sciences, and Engineering, University of Michigan, 2455 Hayward Street, Ann Arbor, MI 48109, USA
[3] Space Science Directorate, Southwest Research Institute, 6220 Culebra Rd., San Antonio, TX 78228, USA
[4] Department of Physics and Astronomy, The University of Texas at San Antonio, San Antonio, TX 78249, USA
[5] Belgian Institute for Space Aeronomy, BIRA-IASB, Ringlaan 3, 1180 Brussels, Belgium
[6] Center for Space and Habitability, University of Bern, Gesellschaftsstrasse 6, 3012 Bern, Switzerland

Received 25 September 2025 / Accepted 4 January 2026

ABSTRACT

Context. Sulphur is chemically versatile and ubiquitous, and important in both planetary and astrochemical processes. Compared to its cosmic abundance, it appears to be significantly depleted in dense interstellar regions – a phenomenon that is the subject of ongoing research. Comets, which retain material from the early Solar System, provide a valuable record for assessing sulphur reservoirs and their isotopic compositions. Comet 67P/Churyumov–Gerasimenko was particularly suitable for in situ investigation.
Aims. This study aims to determine the $^{34}S/^{32}S$ isotopic ratios of CS_2 in comet 67P/Churyumov–Gerasimenko and to investigate if the CS_2 isotopologue double ratio, $^{12}C^{34}S_2/^{12}C^{34}S^{32}S$-to-$^{12}C^{34}S^{32}S/^{12}C^{32}S_2$, is consistent with the statistically expected value.
Methods. We analysed high-resolution spectra acquired by the ROSINA Double Focusing Mass Spectrometer (ROSINA/DFMS) in March 2016, when the Rosetta spacecraft was within 17 km of the nucleus and the CS_2 signal was high. Three CS_2 isotopologues, $^{12}C^{32}S_2$, $^{12}C^{34}S^{32}S$, and $^{12}C^{34}S_2$, were used to derive three $^{34}S/^{32}S$ isotopic ratios.
Results. We report on the first detection of the doubly heavy isotopologue $^{12}C^{34}S_2$ in a comet. All three derived $^{34}S/^{32}S$ ratios yield consistent results, with $\delta^{34}S$ values ranging from $-69.91‰ \pm 42.75‰$ to $-5.49‰ \pm 51.43‰$. These are within 1 to 2σ of the Vienna-Canyon Diablo Troilite (V-CDT) standard, indicating at most a minor depletion in ^{34}S. In contrast to the strong mass-dependent fractionation in water isotopologues measured on 67P – a D_2O/HDO-to-HDO/H_2O ratio of 17, which is far above the equilibrium value of 0.25 – our CS_2 isotopologue double ratio yields 0.2377 ± 0.0139, consistent within 1σ of the statistically expected value of 0.25.

Key words. ISM: abundances – ISM: molecules – comets: individual: 67P/Churyumov–Gerasimenko

1. Introduction

Sulphur is a ubiquitous element found across the Milky Way, and its chemical versatility makes it vital in both planetary chemistry and astrochemistry, influencing climatic processes on planets, like Venus, planetary formation, and astrobiological pathways. Sulphur is continuously produced through explosive oxygen burning in massive stars during their life cycle and subsequently scattered into space by supernovae (Burbidge et al. 1957). In the interstellar medium (ISM), it is the tenth most abundant element and has four stable isotopes: ^{32}S, ^{33}S, ^{34}S, and ^{36}S. In astrochemistry, sulphur-bearing molecules have gained increasing attention in recent decades, particularly in the context of the sulphur depletion problem: in denser and colder regions of the ISM, such as molecular clouds, gas-phase sulphur appears to be depleted by about three orders of magnitude with respect to its cosmic abundance (Tieftrunk et al. 1994). The mechanisms behind this sulphur depletion in star-forming regions are not yet fully understood and are a subject of active investigation, for example through the IRAM GEMS programme (Gas phase Elemental abundances in Molecular Clouds; Fuente et al. 2023) or the PRODIGE large survey observation (PROtostars and DIsks: Global Evolution; Miranzo-Pastor et al. 2025).

A frequent proposition used in astrochemical models is that in these high-density regions the missing sulphur may have been depleted by freezing out onto interstellar dust grains to form H_2S ice via hydrogenation. In the ISM, however, so far only two sulphur-bearing molecules have been securely detected in solid form as ices – OCS (Palumbo et al. 1995, 1997) and SO_2 (Boogert et al. 1997; Zasowski et al. 2009; Rocha et al. 2024) – and their combined observed abundance remains too low (<5% of the cosmic sulphur abundance) to account for all the missing sulphur in cold clouds (Boogert et al. 1997; Palumbo et al. 1997). Even with the increased sensitivity and resolution of the *James Webb* Space Telescope (JWST), solid H_2S has not yet been detected, for example in the dark cloud Chamaeleon I towards NIR38 (McClure et al. 2023).

An alternative sulphur sink could be refractory products of processed H_2S ice, which trap the sulphur: the results of various laboratory experiments where H_2S ice was irradiated via photolysis and/or radiolysis suggest that a substantial fraction of H_2S can be transformed into allotropic forms of sulphur (S_n) up to its most stable S-ring, S_8 (e.g. Jiménez-Escobar & Muñoz Caro 2011; Jiménez-Escobar et al. 2014). Theoretical simulations indicate that this formation of sulphur allotropes may

⋆ Corresponding author: antea.doriot@unibe.ch

be efficient in astrophysical environments (Shingledecker et al. 2020). However, sulphur allotropes are only one out of many possibilities of sulphur-bearing products that may be formed by processing H_2S ice, and the formation efficiency of these products depends sensitively on the initial ice composition. We refer to Mifsud et al. (2021) for a review of laboratory studies performed on interstellar sulphur-containing ice analogues. Despite laboratory experiments and observational results that shed light on the complex sulphur chemistry, it remains a challenge to accurately incorporate sulphur reactions into chemical network models (Laas & Caselli 2019). Isotopes are a way to probe the different reservoirs (both gas- and solid-phase) and explore their inter-connectivities. While chemistry cannot alter the overall isotopic ratio, the specific isotopic ratios in molecules can vary depending on the physical and chemical formation pathways. Hence, isotopic ratios are also helpful for improving the chemical models of these different chemistries. Comets provide a unique window into sulphur chemistry as they are thought to have remained relatively unaltered since their formation in the cold, outer regions of the protoplanetary disk, preserving a record of the chemical composition of the early solar nebula from 4.6 Gyr ago. Therefore, measurements of cometary isotopic ratios offer insights into the conditions prevailing during the formation of molecules in the ISM and trace their chemical evolution from the pre-solar cloud to the protosolar nebula, and later from the protoplanetary disk to their accretion onto solid bodies such as comets (Bockelée-Morvan et al. 2000; Drozdovskaya et al. 2019; López-Gallifa et al. 2024). This is where the in situ study of comets becomes particularly valuable: unlike remote observations, the study of comets in situ opens up the possibility for high-sensitivity and high-precision analyses of refractories and volatiles that are otherwise difficult to detect using remote sensing techniques due to a lack of strong spectral features. Examples are noble gases such as Ar, Kr, and Xe (references in Mousis et al. 2020), or symmetric molecules, for example CS_2, as they lack a permanent dipole moment.

ESA's Rosetta mission, launched in March 2004, is the only mission to date to have accompanied a comet, namely 67P/Churyumov-Gerasimenko (hereafter 67P), on its journey around the Sun. Comet 67P was intensively studied for 25 months, from early August 2014 until the end of September 2016. During this time period, the chemical composition of the cometary coma was continuously measured by the Double Focusing Mass Spectrometer (DFMS), part of the Rosetta Orbiter Spectrometer for Ion and Neutral Analysis (ROSINA) instrument suite (Balsiger et al. 2007). The Rosetta mission revealed a rich chemistry, and a range of complex organic molecules, including aliphatic and aromatic hydrocarbons (Altwegg et al. 2017b; Schuhmann et al. 2019; Hänni et al. 2022), organosulphur compounds (Calmonte et al. 2016; Altwegg et al. 2022; Hänni et al. 2024), ammonium salts (Altwegg et al. 2020b, 2022), and prebiotic chemicals, such as phosphorus and the simplest amino acid, glycine (Altwegg et al. 2016), were detected. Additionally, the mission provided precise isotopic measurements of various elements and compounds, among them silicon (Rubin et al. 2017), krypton (Rubin et al. 2018), xenon (Marty et al. 2017), and chlorine-bearing molecules (Dhooghe et al. 2021), as well as the D/H ratio in water and alkanes (Altwegg et al. 2015; Müller et al. 2022).

For sulphur-bearing species, the $^{34}S/^{32}S$ isotopic ratio was measured for H_2S, OCS, and CS_2 in the gas by Calmonte et al. (2017) and for cometary dust by Paquette et al. (2017). Prior to the in situ Rosetta mission, the isotopic ratio $^{34}S/^{32}S$ in the gas phase had been measured in CS, a remotely observable fragmentation product of CS_2, for several comets: C/1995 O1 (Jewitt et al. 1997), 17P/Holmes (Biver et al. 2008), C/2012 F6, and C/2014 Q2 (Biver et al. 2016). Laboratory work has shown that the formation of CS_2 from CO and H_2S ices is likely (e.g. Ferrante et al. 2008; Garozzo et al. 2010; Chen et al. 2014). CS_2 is also considered a major parent of CS (Jackson et al. 1986), although not the only one (Noonan et al. 2023), as demonstrated by the discrepancy between the results from Rosetta/ROSINA and radio wave spectroscopy (Biver et al. 2023). In addition, CS_2 might also be a parent of S_2 through photodissociation (Li et al. 2021), along with H_2S_2 (Jiménez-Escobar et al. 2012). Determining the isotopic composition of CS_2 will therefore help constrain the chemistry and parent-daughter relationships of sulphur-bearing species in comets.

In this paper, we report on the $^{34}S/^{32}S$ isotopic ratio in CS_2 in comet 67P. For the first time, we also present the isotopic ratio $^{34}S/^{32}S$ derived from the heavy isotopologue $C^{34}S_2$, which enabled us to calculate the double ratio $^{12}C^{34}S_2/^{12}C^{34}S^{32}S$-to-$^{12}C^{34}S^{32}S/^{12}C^{32}S_2$ in analogy to the D_2O/HDO-to-HDO/H_2O double ratio measured by Altwegg et al. (2017b), whose high value indicated low-temperature fractionation during ice formation.

The following sections outline the working principles of DFMS (Sect. 2.1), the data selection and data processing method (Sects. 2.2 and 2.3, respectively), the estimation of uncertainties (Sect. 2.4), and our new findings (Sect. 3), with a summary at the end (Sect. 4).

2. Instrumentation and data evaluation

2.1. Double Focusing Mass Spectrometer

The DFMS of the ROSINA suite is a double focusing mass spectrometer with a high dynamic range of 10^{10} and a mass resolution of $m/\Delta m > 3000$ at 1% peak height on the commanded mass $m/z = 28$ Da/e, while covering the mass range $m/z = 13$–150 Da/e. It can be operated in either of the two basic operation modes – an ion mode for measuring cometary ions or a neutral mode for analysing cometary gases – as well as in one of two resolution modes – high or low resolution. The main ion optical elements of ROSINA/DFMS are: an ionisation box, a transfer lens, an analyser section, a zoom system, and a detector. A detailed description of the ROSINA instrument package is given in Balsiger et al. (2007).

Suitable potentials applied to electrodes in the ionisation box prevents the entry of ambient ions into the instrument in neutral mode while neutral particles can enter the instrument's ionisation box and are ionised by 45 eV electrons, potentially also leading to fragmentation. Most ionised particles are singly charged, and hence we do not explicitly denote the charge unless necessary. Depending on the chosen resolution, a transfer lens focuses the ion beam onto one of two entrance slits of the analyser section: a wide 200 µm slit for low resolution ($m/\Delta m = 800$ at full width at half maximum (FWHM) at $m/z = 28$ Da/e) or a narrow 14 µm slit for high resolution ($m/\Delta m = 5000$ at FWHM at $m/z = 28$ Da/e; De Keyser et al. 2015).

The analyser section has a Nier-Johnson geometry in which the deflection of the ion beam by 90° in the field of the electrostatic analyser is followed by a 60° deflection in the field of the magnetic sector mass analyser. In the former, the ions undergo velocity dispersion, which focuses ions of the same energy. An energy slit placed after the electrostatic analyser filters out ions with undesired energies ($\Delta E/E$ up to 1%). The magnetic sector analyser then disperses the ions based on their momentum

and refocuses ions of the same m/z. A quadrupole-based zoom lens system located behind the analyser section is used to achieve high mass dispersion in high-resolution mode before the ions impact on a position-sensitive focal plane detector.

The ROSINA/DFMS has three independent detectors. Its main detector is a combination of two signal amplifying microchannel plates (MCPs) mounted in Chevron configuration and a linear electron detector array chip (LEDA) with 2 independent detector units (referred to as 'row A' and 'row B') with 512 anodes (or 'pixels') each. The analogue current output of the LEDA chip is digitised by an analogue-to-digital converter returning the signal output as a number of counts per anode (Nevejans et al. 2002). The gain of the MCP system can be varied by applying different potentials to the front and back face of the MCP stack. Sixteen such sets of potentials (called 'gain steps') have been pre-defined (GS1 to GS16) and an automatic gain adjustment algorithm selects the optimal GS for each measurement to maximise the signal without running into saturation. To increase the detection sensitivity of heavy ions ($m/z > 70$ Da/e), an additional post-acceleration bias voltage up to −3 kV is applied at the front face of the MCP (Balsiger et al. 2007).

The continuous operation of ROSINA/DFMS over the course of the mission resulted in a gradual degradation of the gain of the pre-defined gain steps, Similarly, the significant ion peaks, recorded mainly in the centre region of the LEDA chip, led to an uneven degradation of the chip anodes and MCP channels, resulting in a pixel-dependent sensitivity loss. These ageing effects necessitated the introduction of gain correction tables to be used in subsequent data analysis. The latest correction tables have been prepared by Schroeder I et al. (2019) and are included in ESA's Planetary Science Archive (PSA).

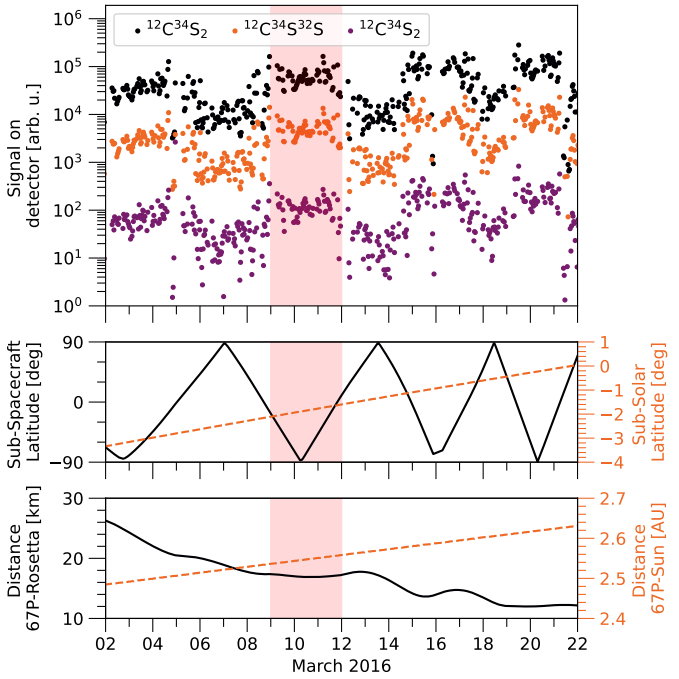

Fig. 1. Some of Rosetta's orbital parameters and the signal strength of the studied CS_2 isotopologues in the vicinity of comet 67P in March 2016. *Top*: signal strength in arbitrary units. *Middle*: sub-spacecraft (solid line) and sub-solar (dashed line) latitudes. *Bottom*: heliocentric (dashed line) distance of 67P and cometocentric distance (solid line) between 67P and the Rosetta spacecraft. The shaded region represents the time period studied in this paper.

2.2. Data selection

In this work, datasets obtained in neutral, high-resolution mode are used to study CS_2 isotopologues, namely $^{12}C^{32}S_2$, $^{12}C^{34}S^{32}S$, and $^{12}C^{34}S_2$ (at commanded masses m/z = 76, 78, and 80 Da/e, respectively). In this mode, the mass range was scanned sequentially from m/z = 13 Da/e up to m/z = 100 Da/e and the acquisition took about 20 s per spectrum. Only data from detector row B were used as their sensitivity was higher than those of row A for the time period studied.

We analysed a total of 183 data files collected between March 9 and 12, 2016, when 67P was at about 2.5 AU from the Sun and the signal of CS_2 was high. Comet 67P was just about a week and a half ahead of its outbound equinox on March 21, 2016 – marking the end of the southern hemisphere's intense summer that lasted about one year. During the studied period, the Rosetta spacecraft was orbiting in the terminator plane at a distance of about 17 km from the comet's centre and almost exclusively measured the southern cometary hemisphere: Going first from −16° sub-spacecraft latitude down to the comet's south pole at −90° before heading back towards the northern hemisphere, crossing the +10° sub-spacecraft latitude mark on March 12, 2016. Figure 1 illustrates the temporal evolution of these orbital parameters in March 2016.

2.3. Data processing

Data analysis begins with pre-processing, which includes the conversion of the digitised LEDA analogue-to-digital converter output per pixel to the number of ions per species per spectrum. This includes application of the pixel-dependent gain and overall MCP gain corrections, and the application of the mass scale. Furthermore, a mass-dependent sensitivity correction is applied. The ROSINA/DFMS data pre-processing procedure is explained in detail in Le Roy et al. (2015) and is performed using an automated code, which takes into account the currently available knowledge of 67P's coma constituents, to facilitate the mass scale determination and to provide an initial rough fit of the prominent peaks. The peak shape is well described by a double Gaussian, i.e. a sum of two Gaussians of which one is about ten times smaller in amplitude and approximately three times broader than the other (Le Roy et al. 2015).

Peaks are initially fitted manually and the obtained parameter values are used as initial values for a subsequent automated constrained minimisation fit using the differential evolution method (Storn & Price 1997). The priors are limited to vary ±20% around their initial value. Additionally, we used the constraint that all peaks on the same spectrum share the same widths and that all double Gaussians on the same spectrum share the same amplitude ratio. In addition, peak centroids coincide with the ions' exact mass. For spectra exhibiting a low signal-to-noise ratio, i.e. for which the peak widths and amplitude ratios cannot be determined with sufficient precision, the values obtained from the previous or subsequent measurement of the same commanded mass are used. If this does not yield satisfying results either, we used the amplitude and width ratios obtained from spectra closest in time that contain one of the other studied isotopologues with a better signal-to-noise ratio, namely spectra containing either $^{12}C^{32}S_2$ (m/z = 76 Da/e) or $^{12}C^{34}S^{32}S$ (m/z = 78 Da/e). The time or mass difference between such measurements is small compared to the large relative statistical uncertainty of the detector counts, so induced uncertainties are negligible.

Table 1. Terrestrial isotope abundances of carbon and sulphur according to Meija et al. (2016).

Isotope	Abundance %
^{12}C	98.8922(28)
^{13}C	1.1078(28)
^{32}S	95.04074(88)
^{33}S	0.74869(60)
^{34}S	4.19599(66)
^{36}S	0.01458(9)

Table 2. Inverse-variance-weighted mean isotopic ratios and deviation from the V-CDT standard value and their associated uncertainty, including statistical and systematic uncertainties, derived in this work for CS_2 in comet 67P.

Isotopic ratio	$^{34}S/^{32}S$ 10^{-2}	σ 10^{-2}	$\delta^{34}S$ ‰	σ ‰
$[^{12}C^{34}S^{32}S/\ ^{12}C^{32}S_2]$	4.3197	0.1565	–21.87	35.44
$[^{12}C^{34}S_2/^{12}C^{34}S^{32}S]$	4.1075	0.1888	–69.91	42.75
$[^{12}C^{34}S_2/^{12}C^{32}S_2]$	4.3921	0.2271	–5.49	51.43

The relative abundance of these isotopologues is obtained by integration of the respective double Gaussian (as obtained from the constrained fit) over all pixels. The peaks of $^{12}C^{34}S_2$ at m/z = 80 Da/e and $^{12}C^{34}S^{32}S$ at m/z = 78 Da/e also contain minor contributions of the isotopologues $^{12}C^{36}S^{32}S$ and $^{13}C^{34}S^{33}S$ (at m/z = 80 Da/e), and $^{13}C^{33}S^{32}S$ and $^{12}C^{33}S_2$ (at m/z = 78 Da/e), respectively, which can neither be resolved by ROSINA/DFMS nor be determined by the data processing procedure, but should be taken into account. Assuming that isotopic abundances on 67P are best described by Meija et al. (2016, cf. our Table 1), the contribution of the unresolvable isotopologues to the respective resolvable peak are calculated to be 9.69% and 0.36% for m/z = 80 Da/e, respectively, and 0.20% and 0.07% for m/z = 78 Da/e, respectively. We subtracted these contributions from the respective integrated peak, noting that within our accuracy only $^{12}C^{36}S^{32}S$ actually makes a perceptible influence.

For each dataset, the isotopic ratio $^{34}S/^{32}S$ was derived from three different, but not independent, ratios of CS_2:

$$\frac{^{34}S}{^{32}S} = \left[\frac{^{12}C^{34}S^{32}S}{^{12}C^{32}S_2}\right] := \frac{1}{2}\frac{^{12}C^{34}S^{32}S}{^{12}C^{32}S_2} \quad (1)$$

$$\frac{^{34}S}{^{32}S} = \left[\frac{^{12}C^{34}S_2}{^{12}C^{34}S^{32}S}\right] := 2\,\frac{^{12}C^{34}S_2}{^{12}C^{34}S^{32}S} \quad (2)$$

$$\frac{^{34}S}{^{32}S} = \left[\frac{^{12}C^{34}S_2}{^{12}C^{32}S_2}\right] := \sqrt{\frac{^{12}C^{34}S_2}{^{12}C^{32}S_2}}. \quad (3)$$

Contributions from isomers are taken into account by the correction factors appearing on the right hand side of Eqs. (1)–(3). Sulphur isotopic ratios are also commonly expressed as deviation from the Vienna-Canyon Diablo Troilite (V-CDT) standard (in per mille):

$$\delta^{34}S = \left(\left[^{34}S/^{32}S\right]_{\text{sample}} / \left[^{34}S/^{32}S\right]_{\text{V-CDT}} - 1\right) \cdot 1000. \quad (4)$$

The currently accepted V-CDT standard value for the sulphur isotopic ratio is $^{34}S/^{32}S$ = 0.044163 (Ding et al. 2001). We obtained mean isotopic ratios for Eqs. (1)–(3), and hence also for Eq. (4), through inverse-variance-weighted averaging over all datasets. Systematic uncertainties were applied to the averaged ratios, which are discussed in the following section.

2.4. Uncertainty

The uncertainty of the isotopic ratio is composed of statistical and systematic uncertainties. The counts registered on the detector follow a Poisson distribution, and thus the associated statistical uncertainty of the count N_p on a specific pixel p is $\propto N_p^{-0.5}$. Fitting uncertainty is taken into account using Gaussian propagation of uncertainty. Inverse-variance-weighted averaging reduces the statistical uncertainties of the isotopic ratios in Eqs. (1)–(3) by –24%, –47%, and –47%, respectively, compared to unweighted averaging. Following Schmelling (1995), the uncertainty of the inverse-variance-weighted mean further incorporates correlations, increasing the statistical error by an additional 31%, 82%, and 72%, respectively.

The pixel-dependent sensitivity-loss correction, compensating the effects of uneven ageing of the LEDA anodes, has an estimated systematic uncertainty of 3% on the averaged ratios of Eqs. (1)–(3), respectively (Calmonte et al. 2017). We estimate the bias introduced by the mass-dependent sensitivity correction to be 2% for Eqs. (1) and (2), and 4% for the ratio in Eq. (3). The correction of the MCP gain steps has an uncertainty of about 6% (Schroeder I et al. 2019). However, since all data were measured on the same MCP gain step, the corresponding systematic uncertainty cancels when calculating isotopic ratios. The systematic uncertainties are added in quadrature to the statistical uncertainties.

3. Results and discussion

It was possible to derive the various $^{34}S/^{32}S$ isotopic ratios, defined by Eqs. (1)–(3), from all spectra analysed.

An excerpt of measured spectra for the commanded masses m/z = 76, 78, and 80 Da/e is shown in Fig. 2. The peaks are well captured by the double Gaussian fits. This holds even for the CS_2 peak on the commanded mass m/z = 80 Da/e, which has a two to three orders of magnitude weaker signal than the CS_2 peaks on the other two commanded masses. It is not possible to resolve the individual contributions of the different CS_2 isotopologues located on the same commanded mass, thus necessitating an estimation of the contributions of the various isotopologues to the peak as discussed in Sect. 2.3.

The individual $^{34}S/^{32}S$ isotopic ratios defined by Eqs. (1)–(3) are shown in Fig. 3 along with their statistical uncertainty (including the fit uncertainty). Correlations between isotopic ratios of the same date of any two panels of Fig. 3 are expected because, for each panel pair, one of the two spectra used to derive the ratios is shared, although this spectrum differs between panel pairs.

The inverse-variance-weighted mean $^{34}S/^{32}S$ isotopic ratios and their total uncertainty (including statistical and systematic uncertainties) are listed in Table 2. Our analysis suggests that the $^{34}S/^{32}S$ isotopic ratios in CS_2 are slightly depleted in the

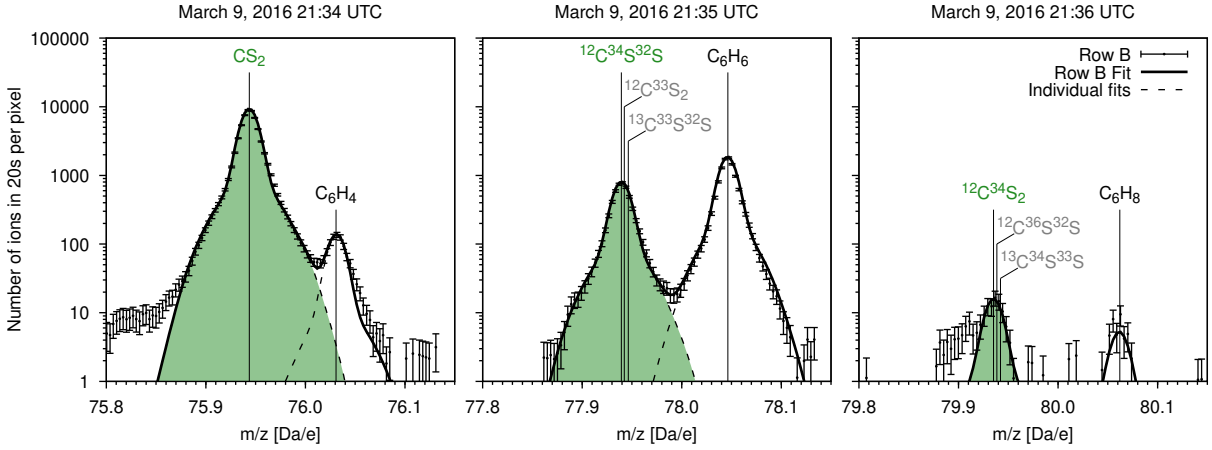

Fig. 2. Example spectra of the mass scans around m/z = 76, 78, and 80 Da/e measured on March 9, 2016. The points depict the pre-processed detector signal of row B. The error bars represent the statistical uncertainty. Individual fits of the detected species (green and black labels) are shown as dashed lines, while the solid line represents the cumulative fit. The signal of the detected CS_2 isotopologues (green label and shaded area) contain minor contributions from other CS_2 isotopologues (labelled in grey) that cannot be resolved with ROSINA/DFMS. Their calculated contributions (see Sect. 2.3) are subsequently subtracted from the integrated signal peak (shaded area). The species' exact ion masses are shown as solid vertical lines.

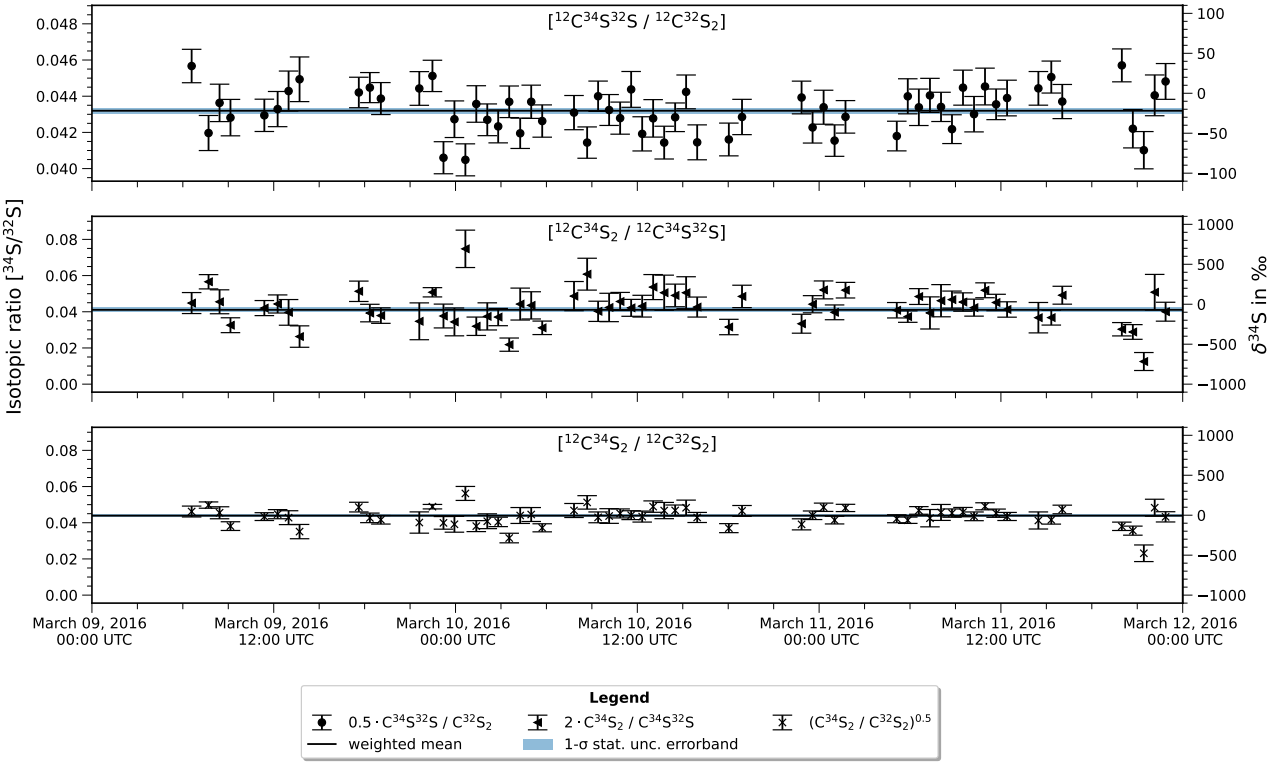

Fig. 3. Isotopic ratios of the individual spectra. On the left axis, the unitless $^{34}S/^{32}S$ ratio is shown, and the right axis represents the corresponding deviation from the V-CDT standard in per mille. Note that the y-axis in the top panel is compressed to one-tenth of the scale used in the remaining panels. The solid line and shaded region represent the weighted mean and its corresponding 1σ statistical error band. The uncertainties of the individual data points shown here only include statistical uncertainties.

heavy ^{34}S isotope ($-70‰ < \delta^{34}S < -5‰$) but are still consistent with the V-CDT standard value within 1σ for the ratios $[^{12}C^{34}S^{32}S/^{12}C^{32}S_2]$ and $[^{12}C^{34}S_2/^{12}C^{32}S_2]$, or within 2σ for the ratio $[^{12}C^{34}S_2/^{12}C^{34}S^{32}S]$.

As we report the first measurement of the doubly substituted isotopologue $^{12}C^{34}S_2$ in a comet, there are no literature values with which we could compare our findings. Moreover, CS_2 is a symmetric molecule lacking a permanent dipole moment, rendering it difficult to observe via remote sensing. Consequently, the closest sulphur-bearing molecule measured remotely in comets and the ISM with which our results can be compared is CS. Figure 4 presents our results along with literature values for comparison. Generally, our results agree well with previously reported sulphur isotopic ratios from cometary studies, including the results from cometary dust measurements of 67P (Paquette et al. 2017). Most measurements fall within 1σ of

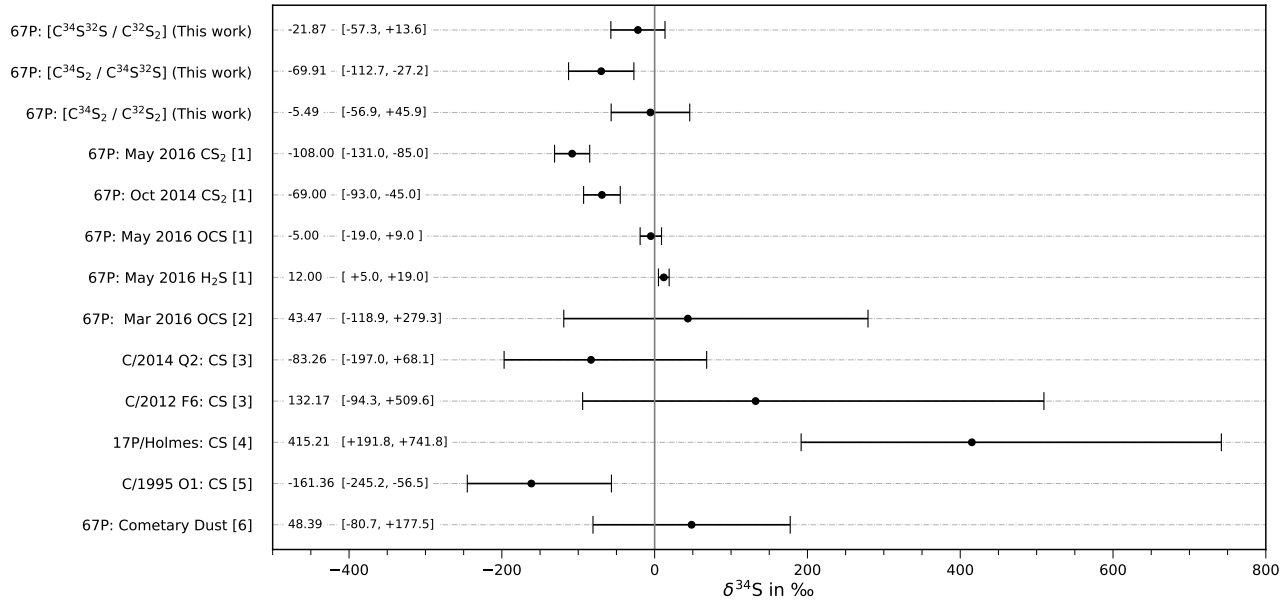

Fig. 4. Compilation of reported cometary values of the $^{34}S/^{32}S$ isotopic ratio (as per mille deviation from the V-CDT standard) and the results of this paper. Error bars include statistical and, if applicable, systematic uncertainties. The numeric values, $x \pm \sigma$, are listed on the left-hand side in the following format: $x \quad [x - \sigma, x + \sigma]$. References: [1] Calmonte et al. (2017), [2] Altwegg et al. (2020a), [3] Biver et al. (2016), [4] Biver et al. (2008), [5] Jewitt et al. (1997), and [6] Paquette et al. (2017).

earlier values, with the exception of the notably high $\delta^{34}S$ value of 415‰ reported for comet 17P/Holmes (Biver et al. 2008). However, it should be noted that this measurement comes with a large uncertainty, namely $\sigma_+ = +326$‰ and $\sigma_- = -223$‰.

Among the results of the Rosetta in situ study, our findings are most directly comparable to those of Calmonte et al. (2017), who analysed sulphur isotopes in multiple species, including CS_2, OCS, and H_2S. Our mean CS_2 isotopologue ratios extracted from the March 2016 measurements ($\delta^{34}S \approx -22‰ \pm 35‰, -70‰ \pm 43‰$, and $-5.5‰ \pm 51‰$; see also Table 2) show a smaller ^{34}S depletion compared to their CS_2 results from both October 2014 ($\delta^{34}S = -69‰ \pm 24‰$) and May 2016 ($\delta^{34}S = -108‰ \pm 23‰$), which is best seen in Fig. 4. In contrast, their May 2016 measurements for OCS and H_2S yielded $\delta^{34}S$ values of $-5‰ \pm 14‰$ and $12‰ \pm 7‰$, respectively – much closer to the terrestrial standard. By comparison, our three CS_2-based ratios exhibit consistent $\delta^{34}S$ values and cluster more tightly around the V-CDT standard, albeit with slightly larger uncertainties. Overall, both our results and those of Calmonte et al. (2017) demonstrate the capability of ROSINA/DFMS to resolve small isotopic deviations at a good accuracy.

Altwegg et al. (2017a) observe a strong mass-dependent fractionation among the deuterated isotopologues of water: They reported a D_2O/HDO-to-HDO/H_2O ratio of 17, far above the expected equilibrium values of 0.25, which is indicative of low-temperature fractionation during ice formation. No such extreme deviation is observed in our results for the CS_2 isotopologues. Calculating the double ratio $^{12}C^{34}S_2/^{12}C^{34}S^{32}S$ to $^{12}C^{34}S^{32}S/^{12}C^{32}S_2$ yields 0.2377 ± 0.0139, which is consistent within 1σ with the statistical expected value of 0.25. This difference between our result and that of Altwegg et al. (2017a) is consistent with expectations: the mass ratio of ^{34}S to ^{32}S is only 1.06, whereas that of D to H is 2. As a result, mass-dependent fractionation effects should be smaller for sulphur-bearing molecules. Our results align with expectations.

Ideally, our results for the sulphur isotopic composition of CS_2 in comet 67P would be compared to other measurements or models of the same molecule to investigate potential links between sulphur isotopic reservoirs, as there could be relative fractionation among reservoirs probed by different molecules. However, such measurements currently do not exist, but some insights can still be gained by comparing with other cometary and interstellar species for which $\delta^{34}S$ is available from the literature. The most direct comparison possible is that discussed above with CS in other comets, as CS is a photodissociation product of CS_2, but only a handful of measurements exist to date. To constrain a potential origin of the sulphur-carrier with a potentially negative $\delta^{34}S$, the cometary results can be compared to measurements in star-forming regions as well as other primitive Solar System matter, such as asteroids and meteorites. Small depletions in the heavy ^{34}S-isotope were observed at temperatures of around 60 K for SO in the Herbig Ae disk Oph-IRS 48 (Booth et al. 2024). SO_2, on the other hand, appears to have a heavy isotope enrichment, albeit with uncertainties related to the opacities of the spectral lines and assumed temperatures, that is not consistent with the SO_2 in 67P (Altwegg et al. 2020a). This could indicate that the cometary sulphur in CS_2 could share an isotopic signature with at least one disk sulphur component probed by SO, while it is inconsistent with the one reflected in SO_2, but additional measurements will be needed to clarify whether a potential isotopic link exists. Booth et al. (2024) argue that the sulphur seen in the Oph-IRS 48 disk could be linked to UV photochemistry or shocks. Laboratory studies for vacuum ultraviolet irradiation of H_2S are available from Chakraborty et al. (2013), yielding a range of isotopic compositions, but rarely to negative $\delta^{34}S$, which renders photochemistry linked to H_2S a less likely scenario for the CS_2 in 67P. A negative $\delta^{34}S$ value is reported for one of the two surface samples ($\delta^{34}S = -3.0‰ \pm 2.3‰$ for A0106 and $\delta^{34}S = -1.10‰ \pm 1.62‰$ for C107) obtained by the Hayabusa-2 mission from two different locations on asteroid Ryugu (Yoshimura et al. 2023). The similarity of these values

with the cometary results could point towards a shared sulphur isotopic reservoir among primitive Solar System bodies like asteroids and comets if confirmed, although the asteroidal sulphur carriers might be affected by aqueous alteration (e.g. Takano et al. 2024). The variations in δ^{34}S are generally small for meteorites except carbonaceous chondrites, which show a slightly wider spread of values, including negative ones (e.g. Labidi et al. 2017; Alexander et al. 2022). However, establishing a link between meteoritic and cometary reservoirs requires a more thorough understanding of the sulphur carriers, which is an active topic of ongoing research (e.g. Herath et al. 2025). In addition to providing a value for comparison with future in situ, remote, or laboratory measurements, the results presented here can also serve as input data for future chemical models of sulphur isotopic networks, similar to those already available for other stable isotopes (e.g. Colzi et al. 2020; Loison et al. 2019a,b, 2020; Sipilä et al. 2023) to progress the understanding of chemical links among sulphur reservoirs.

4. Summary

We have presented high-resolution in situ measurements of the $^{34}S/^{32}S$ isotopic ratio in CS_2 in comet 67P using data from the ROSINA/DFMS instrument aboard ESA's Rosetta spacecraft. Our analysis covers the period of March 9–12, 2016, when the spacecraft was orbiting approximately 17 km from the comet nucleus and the CS_2 signal was strong.

For the first time in a comet, the doubly heavy isotopologue $^{12}C^{34}S_2$ was detected, allowing us to derive the $^{34}S/^{32}S$ ratio using three different isotopologue ratios: $^{12}C^{34}S^{32}S/^{12}C^{32}S_2$, $^{12}C^{34}S_2/^{12}C^{34}S^{32}S$, and $^{12}C^{34}S_2/^{12}C^{32}S_2$. All three isotopic ratios yield consistent results, with δ^{34}S values ranging from $-69.91‰ \pm 42.75‰$ to $-5.49‰ \pm 51.43‰$ relative to the V-CDT standard. These values indicate at most a slight depletion in ^{34}S, as they are still consistent with V-CDT within 1 to 2σ. They are also in good agreement with prior CS_2 measurements for 67P from Calmonte et al. (2017) and are broadly consistent with results from CS measured earlier in other comets. In contrast to the pronounced mass-dependent fractionation observed in water isotopologues (Altwegg et al. 2017a), the CS_2 double isotopic ratio $^{12}C^{34}S_2/^{12}C^{34}S^{32}S$-over-$^{12}C^{34}S^{32}S/^{12}C^{32}S_2$ of 0.2377 ± 0.0139 conforms with the statistically expected value of 0.25.

The sulphur isotopic composition of CS_2 in comet 67P provides tentative constraints on its potential origin. Observations of sulphur-bearing species in the Herbig Ae disk Oph-IRS 48 (Booth et al. 2024) suggest that at least one sulphur component traced by SO could share a similar isotopic signature at 60 K, whereas the isotopic signature of SO_2 appears inconsistent. In addition, the similarity between the δ^{34}S values measured in comet 67P and those from surface samples of asteroid Ryugu (Hayabusa-2 mission; Yoshimura et al. 2023) may indicate a shared sulphur isotopic reservoir. However, these constraints remain tentative and require additional measurements and a more thorough understanding of the sulphur carriers for confirmation.

In addition to providing a value for comparison with future in situ, remote, or laboratory measurements, the results presented here can also serve as input data for chemical models of sulphur isotopic networks, helping advance the understanding of chemical links among sulphur reservoirs. Future work could focus on expanding such analyses to other volatile sulphur species and comparing isotopic ratios among comets and in the ISM to further explore the chemical diversity and origins of volatile reservoirs. For example, new laboratory work on the IR spectra of CS_2 (Taillard et al. 2025) may now also pave the way for a detection in interstellar ices.

Acknowledgements. ROSINA would not give such outstanding results without the work of the many engineers, technicians, and scientists involved in the mission, in the Rosetta spacecraft, and in the ROSINA instrument team over the last 20 yr, whose contributions are gratefully acknowledged. Rosetta is a European Space Agency (ESA) mission with contributions from its member states and NASA. We acknowledge herewith the work of the whole ESA Rosetta team. The work by A.C.D., R.B., N.H., D.R.M., and M.R. was funded by the Canton of Bern and the Swiss National Science Foundation (SNSF_200020_182418). S.F.W. acknowledges support of the SNSF Eccellenza Professorial Fellowship PCEFP2_181150. M.R.C. acknowledges the financial support provided by the NASA grant 80NSSC20K0651.

References

Alexander, C. M. O., Wynn, J. G., Bowden, R., & Scott, E. 2022, Meteorit. Planet. Sci., 57, 334
Altwegg, K., Balsiger, H., Bar-Nun, A., et al. 2015, Science, 347, 1261952
Altwegg, K., Balsiger, H., Bar-Nun, A., et al. 2016, Sci. Adv., 2, e1600285
Altwegg, K., Balsiger, H., Berthelier, J. J., et al. 2017a, Phil. Trans. R. Soc. A, 375, 20160253
Altwegg, K., Balsiger, H., Berthelier, J. J., et al. 2017b, MNRAS, 469, S130
Altwegg, K., Balsiger, H., & Fuselier, S. A. 2019, Annu. Rev. Astron. Astrophys., 57, 113
Altwegg, K., Balsiger, H., Combi, M., et al. 2020a, MNRAS, 498, 5855
Altwegg, K., Balsiger, H., Hänni, N., et al. 2020b, Nat. Astron., 4, 533
Altwegg, K., Combi, M., Fuselier, S. A., et al. 2022, MNRAS, 516, 3900
Balsiger, H., Altwegg, K., Bochsler, P., et al. 2007, Space Sci. Rev., 128, 745
Biver, N., Bockelée-Morvan, D., Wiesemeyer, H., et al. 2008, in LPI Contributions, 1405, ACM 2008, ed. LPI Editorial Board, 8146
Biver, N., Moreno, R., Bockelée-Morvan, D., et al. 2016, A&A, 589, A78
Bockelée-Morvan, D., Lis, D. C., Wink, J. E., et al. 2000, A&A, 353, 1101
Biver, N., Bockelée-Morvan, D., Crovisier, J., et al. 2023, A&A, 672, A170
Boogert, A. C. A., Schutte, W. A., Helmich, F. P., Tielens, A. G. G. M., & Wooden, D. H. 1997, A&A, 317, 929
Booth, A. S., Drozdovskaya, M. N., Temmink, M., et al. 2024, ApJ, 975, 72
Burbidge, E. M., Burbidge, G. R., Fowler, W. A., & Hoyle, F. 1957, RPM, 29, 547
Calmonte, U., Altwegg, K., Balsiger, H., et al. 2016, MNRAS, 462, S253
Calmonte, U., Altwegg, K., Balsiger, H., et al. 2017, MNRAS, 469, S787
Chakraborty, S., Jackson, T. L., Ahmed, M., & Thiemens, M. H. 2013, Proc. Natl. Acad. Sci. U.S.A., 110, 17650
Chen, Y.-J., Juang, K.-J., Nuevo, M., et al. 2014, ApJ, 798, 80
Colzi, L., Sipilä, O., Roueff, E., Caselli, P., & Fontani, F. 2020, A&A, 640, A51
De Keyser, J., Dhooghe, F., Gibbons, A., et al. 2015, Int. J. Mass Spectrom., 393, 41
Dhooghe, F., De Keyser, J., Hänni, N., et al. 2021, MNRAS, 508, 1020
Ding, T., Valkiers, S., Kipphardt, H., et al. 2001, Geochim. Cosmochim. Acta, 65, 2433
Drozdovskaya, M. N., van Dishoeck, E. F., Rubin, M., Jørgensen, J. K., & Altwegg, K. 2019, MNRAS, 490, 50
Ferrante, R. F., Moore, M. H., Spiliotis, M. M., & Hudson, R. L. 2008, ApJ, 684, 1210
Fuente, A., Rivière-Marichalar, P., Beitia-Antero, L., et al. 2023, A&A, 670, A114
Garozzo, M., Fulvio, D., Kanuchova, Z., Palumbo, M. E., & Strazzulla, G. 2010, Astron. Astrophys., 509, A67
Grim, R. J. A., & Greenberg, J. M. 1987, A&A, 181, 155
Hänni, N., Altwegg, K., Combi, M., et al. 2022, Nat. Commun., 13, 3639
Hänni, N., Altwegg, K., Baklouti, D., et al. 2023, A&A, 678, A22
Hänni, N., Altwegg, K., Combi, M., et al. 2024, ApJ, 976, 74
Hässig, M., Altwegg, K., Balsiger, H., et al. 2017, A&A, 605, A50
Herath, A., McAnally, M., Turner, A. M., et al. 2025, Nat. Commun., 16, 5571
Jackson, W. M., Butterworth, P. S., & Ballard, D. 1986, ApJ, 304, 515
Jewitt, D. C., Matthews, H. E., Owen, T., & Meier, R. 1997, Science, 278, 90
Jiménez-Escobar, A., & Muñoz Caro, G. M. 2011, A&A, 536, A91
Jiménez-Escobar, A., Muñoz Caro, G. M., Ciaravella, A., et al. 2012, ApJ, 751, L40
Jiménez-Escobar, A., Muñoz Caro, G. M., & Chen, Y. J. 2014, MNRAS, 443, 343
Laas, J. C., & Caselli, P. 2019, A&A, 624, A108

Labidi, J., Farquhar, J., Alexander, C. M. O. D., Eldridge, D. L., & Oduro, H. 2017, Geochim. Cosmochim. Acta, 196, 326
Le Roy, L., Altwegg, K., Balsiger, H., et al. 2015, A&A, 583, A1
Li, Z., Zhao, M., Xie, T., et al. 2021, J. Phys. Chem. Lett., 12, 844
Lodders, K., Bergemann, M., & Palme, H. 2025, Space Sci. Rev., 221, 23
Loison, J.-C., Wakelam, V., Gratier, P., & Hickson, K. M. 2019a, MNRAS, 484, 2747
Loison, J.-C., Wakelam, V., Gratier, P., et al. 2019b, MNRAS, 485, 5777
Loison, J.-C., Wakelam, V., Gratier, P., & Hickson, K. M. 2020, MNRAS, 498, 4663
López-Gallifa, Á., Rivilla, V. M., Beltrán, M. T., et al. 2024, MNRAS, 529, 3244
Marty, B., Altwegg, K., Balsiger, H., et al. 2017, Science, 356, 1069
McClure, M. K., Rocha, W. R. M., Pontoppidan, K. M., et al. 2023, Nat. Astron., 7, 431
Meija, J., Coplen, T., Berglund, M., et al. 2016, Pure Appl. Chem., 88, 293
Mifsud, D. V., Kaňuchová, Z., Herczku, P., et al. 2021, Space Sci. Rev., 217, 14
Miranzo-Pastor, J. J., Fuente, A., Navarro-Almaida, D., et al. 2025, A&A, 700, A251
Mousis, O., Aguichine, A., Atkinson, D. H., et al. 2020, Space Sci. Rev., 216, 77
Müller, D. R., Altwegg, K., Berthelier, J. J., et al. 2022, A&A, 662, A69
Nevejans, D., Neefs, E., Kavadias, S., Merken, P., & Van Hoof, C. 2002, Int. J. Mass Spectrom., 215, 77
Noonan, J. W., Parker, J. W., Harris, W. M., et al. 2023, Planet. Sci. J., 4, 73
Palumbo, M. E., Tielens, A. G. G. M., & Tokunaga, A. T. 1995, ApJ, 449, 674
Palumbo, M. E., Geballe, T. R., & Tielens, A. G. G. M. 1997, ApJ, 479, 839
Paquette, J. A., Hornung, K., Stenzel, O. J., et al. 2017, MNRAS, 469, S230
Rocha, W. R. M., van Dishoeck, E. F., Ressler, M. E., et al. 2024, A&A, 683, A124
Rubin, M., Altwegg, K., Balsiger, H., et al. 2017, A&A, 601, A123
Rubin, M., Altwegg, K., Balsiger, H., et al. 2018, Sci. Adv., 4, eaar6297
Ruffle, D. P., Hartquist, T. W., Caselli, P., & Williams, D. A. 1999, MNRAS, 306, 691
Schmelling, M. 1995, Phys. Scr., 51, 676
Schroeder I, I. R. H. G., Altwegg, K., Balsiger, H., et al. 2019, A&A, 630, A29
Schuhmann, M., Altwegg, K., Balsiger, H., et al. 2019, A&A, 630, A31
Shingledecker, C. N., Lamberts, T., Laas, J. C., et al. 2020, ApJ, 888, 52
Sipilä, O., Colzi, L., Roueff, E., et al. 2023, A&A, 678, A120
Storn, R., & Price, K. V. 1997, J. Glob. Optim., 11, 341
Taillard, A., Martín-Doménech, R., Carrascosa, H., et al. 2025, Astron. Astrophys., 694, A263
Takano, Y., Naraoka, H., Dworkin, J. P., et al. 2024, Nat. Commun., 15, 5708
Tieftrunk, A., Pineau des Forets, G., Schilke, P., & Walmsley, C. M. 1994, A&A, 289, 579
Yoshimura, T., Takano, Y., Naraoka, H., et al. 2023, Nat. Commun., 14, 5284
Zasowski, G., Kemper, F., Watson, D. M., et al. 2009, ApJ, 694, 459